

Seismic behavior of steel column-base-connection equipped by NiTi shape memory alloy

Reza Jamalpour^{1a}, Masoud Nekooei^{*1} and Abdolreza Sarvghad Moghadam^{2b}

¹Department of Civil Engineering, Science and Research Branch, Islamic Azad University, Tehran, Iran

²International Institute of Earthquake Engineering and Seismology (IIEES), Tehran, Iran

(Received June 28, 2016, Revised June 21, 2017, Accepted July 31, 2017)

Abstract. The behavior of moment resistant steel structures depends on both the beam-column connections and columns foundations connections. Obviously, if the connections can meet the adequate ductility and resistance against lateral loads, the seismic capacity of these structures will be linked practically to the performance of these connections. The shape memory alloys (SMAs) have been most recently used as a means of energy dissipation in buildings. The main approach adopted by researchers in the use of such alloys is firstly bracing, and secondly connecting the beams to columns. Additionally, the behavior of these alloys is modeled in software applications rarely involving equivalent torsional springs and column-foundation connections. This paper attempts to introduce the shape memory alloys and their applications in steel structural connections, proposing a new steel column- foundation connection, not merely a theoretical model but practically a realistic and applicable model in structures. Moreover, it entails the same functionality as macro modeling software based on real behavior, which can use different materials to establish a connection between the columns and foundations. In this paper, the suggested steel column-foundation connection was introduced. Moreover, exploring the seismic dynamic behavior under cyclic loading protocols and the famous earthquake records with different materials such as steel and interconnection equipment by superelastic shape memory alloys have been investigated. Then, the results were compared to demonstrate that such connections are ideal against the seismic behavior and energy dissipation.

Keywords: SMA; steel column-base-connection; cyclic/seismic behavior; energy dissipation

1. Introduction

One of the resistant structures against lateral loads is moment resistant frame (MRF) in which the beams and columns form a moment frame through a fixed support in connections. The behavior of flexural steel structures largely depends on the performance of column-beam connections. Because of this importance, recently many researchers have focused their investigation on beam to column connection and behavior of MRFs. Experimental results of three Reduced Beam Section Tubular TW-RBS connections under cyclic loading have been conducted (Saleh *et al.* 2016). The load transfer mechanism and load-bearing capacity of cast steel joints for H-shaped beam to square tube column connection based on the deformation compatibility theory are studied (Han *et al.* 2015). The optimum design of planar frames with semi-rigid connections by standard sections from (AISC) table has been studied (Artar *et al.* 2015). Steel bolted connection and bolts saturation on connection plate for high strength steel

connections built up with high strength bolts have been investigated (Öztekın 2015). However, in such systems, the structural joints should be designed to provide structural members and connections with adequate ductility and resistance against lateral load. Basically, the lateral resistance and ductility capacity of connections in flexural structures are one of the most essential factors contributing to the seismic capacity of these structures. The study on sample frames in Fig. 1 demonstrated that lateral forces supported by the moment frame depend not only on beam-to-column connections, but also columns foundations connections. The sample frames showed different performances only due to differences in how columns are connected to the foundations. In case the connections can meet the adequate ductility and resistance against lateral loads similar to beam-column connections, the seismic capacity of these structures will be linked practically to the performance of these connections.

The designer is in charge of deciding how to connect the columns to foundations as well as on the performance of the structure, this can develop on the basis of a controlled connection scheme, Fig. 2, functioning similar to fixed connection if it entails infinite rotational stiffness and in the absence of rotational stiffness, it will function similar to a hinge connection, where the right materials can be used to achieve great performance under cyclic and seismic loading. The special dynamic performance of controlled connection requires the special properties of elasticity, resistance against large strains, energy dissipation,

*Corresponding author, Assistant Professor

E-mail: msnekooei@gmail.com

^aPh.D.

E-mail: jamalpour_reza@kiauo.ac.ir

^bAssociate Professor

E-mail: moghadam@iiees.ac.ir

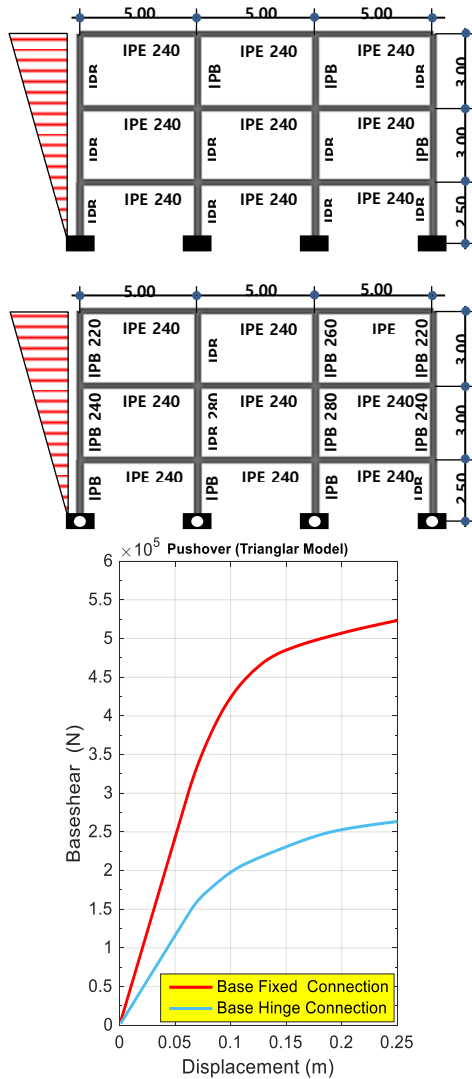


Fig. 1 Behavior of MRF in pushover analysis with Hinge and fixed column-foundation connections

reversibility, etc. Applying the appropriate contrivances in the connections, the lateral stiffness and ductility of steel flexural structures (seismic-induced energy dissipation capability) can be improved in addition to the seismic elements such as type and technical characteristics, stiffness, damping and so on). Hence, the application of appropriate connections with great ductility, attenuation and energy absorption can certainly improve the structural performance on base stimulation.

Therefore, the dynamic controlled behavior of these connections strongly requires the use of special materials. Nowadays, these materials are known as shape memory alloys (SMAs).

2. Introducing the Shape Memory Alloy (SMA) and its behavior

Shape memory alloys are exotic materials with magical properties under visible permanent deformations by up to 10% or more. In addition, they entail metallic properties

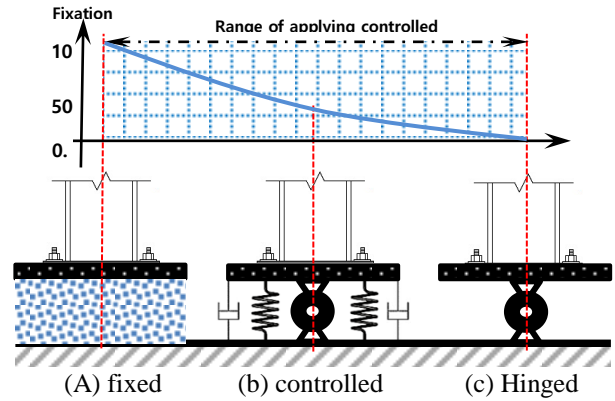
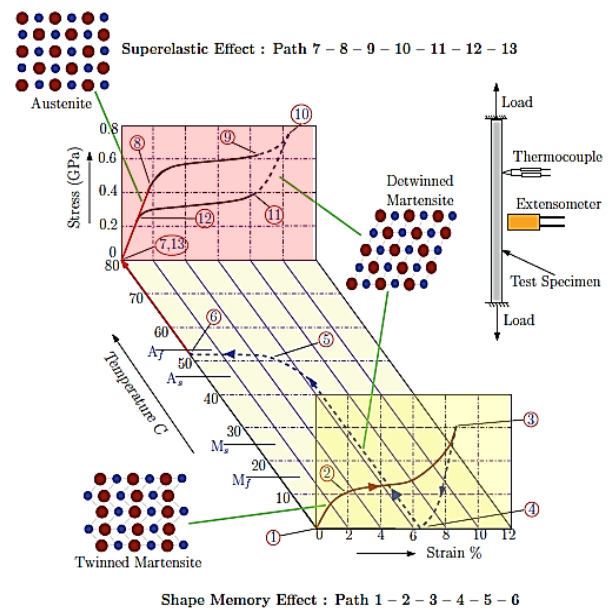


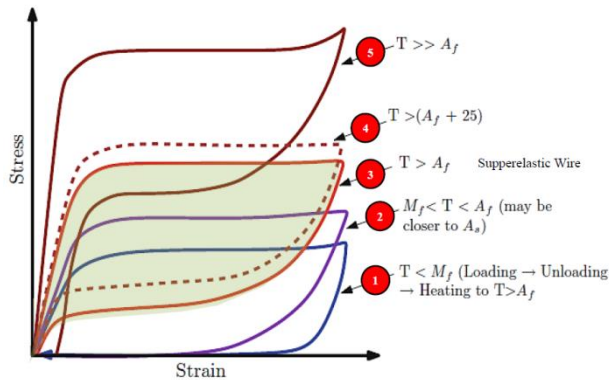
Fig. 2 Schematic view of controlled column-foundation connections and the scope of application



Shape memory effect (Path 6-1) and superelastic effect(Path 13-7) can be seen. This reversibility effect is a manifestation of solid-phase transformations between a stable austenitic phase, high-temperature phase and low-temperature martensitic phase.

Fig. 3 3D temperature-stress-strain diagram describing a thermo-mechanical test(Ashwin Rao *et al* 2015).

such as strength, stiffness, high expenditure, cast ability and so on (Lecce *et al.* 2015). In recent decades, a great deal of research in civil engineering and structural engineering have been focused on using intelligent systems in civil development projects with an emphasis on structural response control against vibration and seismic waves. A Hybrid device consists of two main components; self-centering wires of shape memory alloy (SMA) and steel pipe section as an energy dissipater element has been used in steel braced frames to control Seismic response (Salari *et al.* 2015). Many innovative tools and systems have been proposed mainly using shape memory alloys based on Nitinol and copper so as to absorb some of the energy loss caused by earthquakes and dampen the earthquake forces aimed at structural retrofitting. Shape memory alloys have



Curve (1) The Response of the wire under the influence of temperature lower than M_f after it was unloaded and achieved zero stress. The shape memory property was achieved by heating the wire above the A_f .

Curve (2) The response of the wire above the temperature $M_f < T < A_f$, which is almost identical to A_s .

Curve (3) Displays the classic superelastic wire above A_f .

Curve (4) Displays the temperature-dependent superelastic wire.

Curve (5) The response of the temperatures far higher than A_f .

Fig. 4 Response of SMA wire under different temperature regimes (Ashwin Rao *et al.* 2015)

two outstanding features including a shape memory and superelastic behavior. The shape memory alloys are capable of bouncing back to a preset shape when heating up over the characteristic temperature of austenite transformation (A_f). They are also capable of high strain recovery (about 8%). The stress-strain hysteresis due to mechanical loading-unloading under isothermal conditions is known as superelastic effect. Fig. 3 illustrates the conventional shape memory effect on a path (1 to 6) and the superelastic effect on a path (7 to 13) on temperature-stress-strain diagram (Rao *et al.* 2015). In response to superelastic shape memory alloys, the phase transformations lead to nonlinear hysteresis reaction. This has given such materials superior properties in energy dissipation as an excellent option for damper materials. Due to the different crystal structures of austenite and martensite, the shape memory alloys lead to different superelastic responses in various parts, being sensitive to operating temperature. Fig. 4 displays the performance of a superelastic wire sample at different temperatures. The classic Nitinol superelastic wires and rods are among shape memory alloy applicable in structural connections as adopted in the current paper. Many innovative tools and systems have been proposed mainly using shape memory alloys based on Nitinol and copper so as to absorb some of the energy loss caused by earthquakes and damped the earthquake forces aimed at structural retrofitting. The variable stiffness in superelastic behavior can be used to control the force and displacement in three different strain scenarios. At strains lower than 1%, the austenite modulus of elasticity can be employed to limit the strains. In the middle strain levels more than 1% and less than 6%, the reduced modulus can be used to limit the force

transferred to the structure, even if there is a large displacement.

In large strains more than 6%, the increased modulus in stress-induced martensitic phase can be used to control displacement under earthquake induced stress conditions. By the load removal, the low-stress path in reverse transfer leads to the hysteresis energy loss, which is a desirable feature control the vibrations exerted on structures. Furthermore, the superelastic behavior provides the use of austenite elements to self-centering property of shape memory alloys. In fact, they obtain the original shape after deformation caused by stress or temperature.

3. Literature review

Structural connection or beam-column connections are vulnerable during earthquakes. Prior to the 1990s, resistant steel structures composed of beam-column connections were considered for a long time as a desirable system for encounter the earthquake-induced forces. However, the Northridge earthquake in 1994 witnessed the failure of these connections, followed by numerous investigations to strengthen the connections. To deal with this issue and cost-effective reduction of repair processes, the high-strength prestressed rods were applied on connections so as to reach a good self-centering mechanism. Many researchers proposed the adoption of shape memory alloy systems because of the potential to create a simple, flexible centripetal mechanism and unique ability to self-restore strain as much as 8%. This was used to control the frequency response of connections under high-vibration earthquake, especially in steel structures. Their laboratory studies on beam-column connections, Fig. 5 at actual scale with and without Nitinol tendons reported (Leon *et al.* 2001). The tendons were designed to act in shape memory mode (martensite behavior). At the end of the cycle, they were heated until the connection restored to its original status. Drawn after the periodic stains by 4%, the hysteresis loops were almost identical. As a result, the connection containing a shape memory alloy was capable of tolerating the constant deformation without diminishing in resistance. Taking advantage of the same shape memory effect tested a steel beam to column connection through Nitinol shape memory alloy strains under periodic and sequential quasi-static loads (Ocel *et al.* 2004). This connection was composed of four Nitinol shape memory rods linking the upper and lower flanges to the column's flange acting as an initial torque transfer mechanism. After heating the tendons, the displacement of residual on beam's top was recycled up to 76% and the reconnection was tested, indicating the repetitive behavior and stability of energy dissipation. The sample connection explored with the initial strain using four shape memory aluminum-beryllium-copper rods with a diameter of 3 mm (Sepulveda *et al.* 2011). The proposed structure consisted of end plate connection between a hollow structural beam and a wide flange steel column. The shape memory rods in austenitic phase were used to strengthen the end plate on the column's flange. The laboratory results showed that the beam-column connection

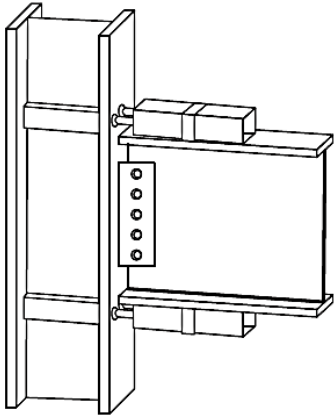


Fig. 5 Beam-column connection in tests conducted by (Leon *et al.* 2001)

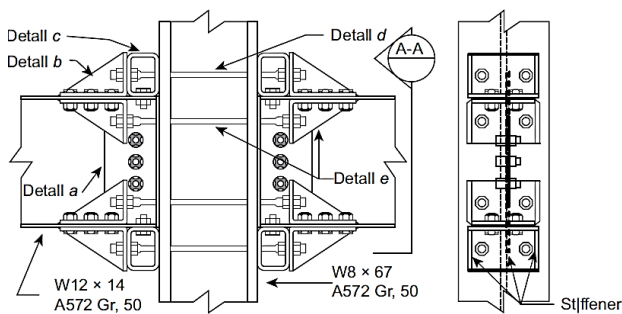


Fig. 6 Beam-column connection in tests conducted by (Speichers *et al.* 2011)

indicated little superelastic behavior, balanced energy dissipation and strength drop after going through multiple cycles of 3% relative displacements.

The comparative studies conducted on interior beam-column connections Fig. 6, using (1) steel tendons, (2) martensitic Nitinol shape memory alloys and (3) superelastic Nitinol shape memory alloy and parallel aluminum (Speichers *et al.* 2011). The superelastic shape memory alloy connections were capable of 85% transformation after a relative deformation of 5%, providing the concentration of all non-elastic deformations on the tendons when the other system components were in elastic mode.

Exposure assessment to seismic vibrations in steel MRF in the beam-column connections in two types of elements contains shape memory alloy rods with large diameters, using (1) superelastic shape memory elements with self-centering capability (2) martensitic shape memory elements with high energy dissipation, Fig. 7 has been tested (Desroches *et al.* 2010). For this purpose, two steel structures (three and nine floors) were employed to demonstrate the capabilities of connections optimized by shape memory alloys on a large structure. Numerous tests showed that the shape memory alloy energy-dissipating connections were more effective in reducing maximum deformation, whereas connections involving superelastic shape memory alloys were more ideal to curtail the residual deformations.

The seismic behavior of steel structural models with

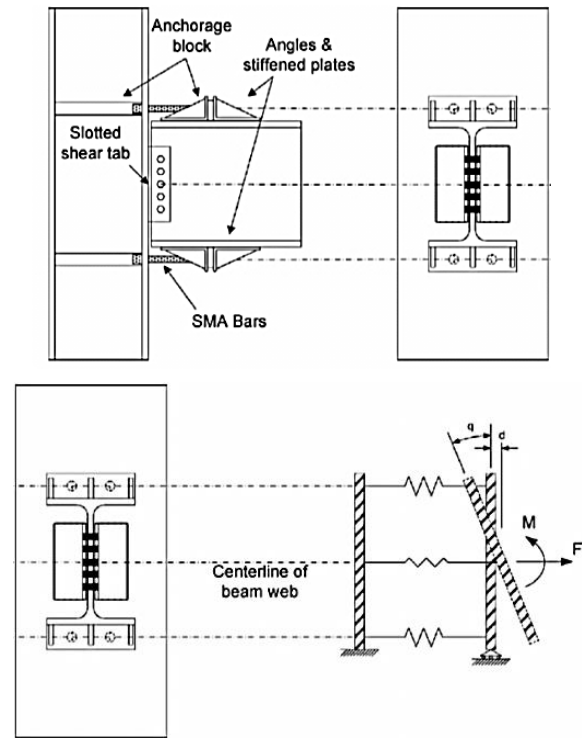


Fig. 7 Model provided for connection involving shape memory alloy (Desroches *et al.* 2011)

different numbers of floors are taken into account and connection with shape memory alloys in the austenite phase so as to explore the rotation behavior of connections was tested (Rafooei *et al.* 2011). The relevant innovative connection between steel beams and columns were filled with concrete. Many studies also noted that bolted connections properly designed with the correct details can improve performance concerning earthquake resistance, ductility and rigidity (Hu *et al.* 2011). An innovative connection composed of an end plate and screws containing shape memory alloys, continuity plates, flange stiffener and web stiffener investigated (Ma *et al.* 2007). This innovative connection proved great seismic performance because its need for energy dissipation and ductility were fulfilled by modifying the shape memory screws. In this case, the plastic hinge is formed inside the connection, while the structural components (e.g., beams, columns and end plate) largely remain constant within the elastic range. The resulting benefits include minimizing the repair operations after the earthquake and the costs related to the structural components. This concept was deeply investigated. (Fang *et al.* 2014). They studied the cyclic performance of end plate connections through normal shape memory alloy screws with high strength Fig. 8. The shape memory connectors demonstrated excellent self-centering and balanced energy dissipation capacity with vibration dampening by up to 17.5%. The typical end plate connections with high-strength bolts showed great energy dissipation capacity and ductility, even though deformation was permanent. In addition, all end plates acted as a thick plate in the shape memory alloy screw connection, where there was not any non-elastic deformation. When the length and diameter of the screw

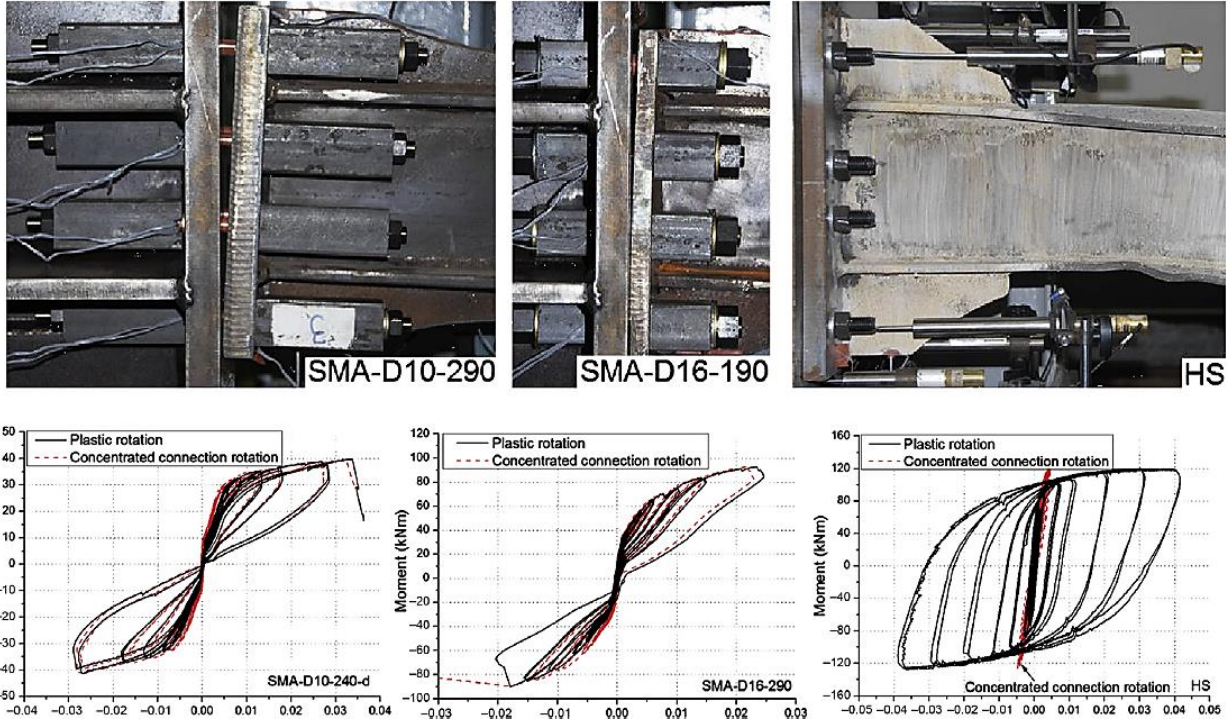
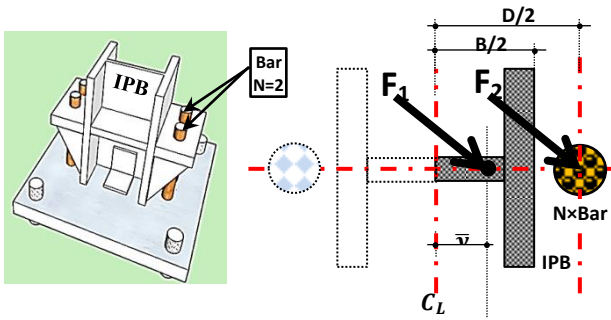

 Fig. 8 model provided for connection involving shape memory alloy screws (Fang *et al.* 2014)


Fig. 9 Parameters for calculating area and number of rods for bearing of bending moments

was changing the behavior of connections, skinny screws (long screws with small diameter) demonstrated higher plasticity and better hysteresis stability.

4. Suggested connection

The schematic view of fixed column-foundation connection in Fig. 9 is considered. It is assumed that the axial strain and stress caused by axial force in the column is tolerated by the base plate and foundation, where the column can rotate as the moment on the column at the support zone is tolerated by the couple in the tie rod shown on the Fig. 9.

$$\begin{aligned} F_1 &= \frac{1}{2} \times \frac{1}{2} A_{IPB} \times \sigma_{yIPB} \\ F_2 &= N \times A_{Bar} \times \sigma_{yBar} \end{aligned} \quad (1)$$

Assume an IPB for the column, different materials for columns and rods are used. Assume triangular stress

distribution on cross-section is accrued from flange outside the edge of column with entire plastic stress towards natural axis of IPB with zero, so the equivalent diameter of rods Φ_{bar} can be calculated according to Eq. (2).

$$\Phi_{bar} = \sqrt{\frac{2}{\pi \times N \times D} \times \frac{\sigma_{yIPB}}{\sigma_{yBar}} \times \left[\left(\frac{B}{2} - t_f \right)^2 \times t_w + 2 \times \left(\frac{B}{2} - \frac{t_f}{2} \right) \times (b_f, t_f) \right]} \quad (2)$$

Where the parameters include:

Φ_{bar} = Equivalent rod diameter used to bear moment on the connection.

A_{bar} = Rod cross-section used to bear moment on the connection.

σ_{yBar} = Rod yield stress used to bear moment on the connection.

N = Number of rods used to bear moment on the connection on each side.

B = Height of IPB (web height in addition to the thickness of flanges).

D = Height of IPB plus distance between rod and flanges, $D = B + 2 \times (5 \sim 10) \text{ cm}$

b_f = Width of profile flange (IPB).

t_f = Thickness of profiles flange (IPB).

t_w = Thickness of profile web (IPB).

σ_{yIPB} = Profile yield stress (IPB).

The Φ_{bar} for a few profiles can be obtained from Table 1 based on IPBL and in terms of number of rods needed for different types of steel according to Eq. (2), diameters of equivalent rods.

The free length of the rod before buckling can be calculated in terms of diameter and materials according to

Table 1 Equivalent diameters of rods for IPB_N (made of different materials), $D \approx 10^{\text{cm}}$

IPB	$\Phi_{\text{bar}} \text{ (mm)}$								
	$\sigma_{y\text{Bar}} \approx 240 \text{ mpa}$			$\sigma_{y\text{Bar}} \approx 300 \text{ mpa}$			$\sigma_{y\text{Bar}} \approx 640 \text{ mpa}$		
	N_{bar}			N_{bar}			N_{bar}		
	2	3	4	2	3	4	2	3	4
160	30	25	21	27	22	19	19	15	13
180	32	26	23	29	23	20	20	16	14
200	35	28	24	31	25	22	21	17	15
220	37	31	26	33	27	24	23	19	16
240	40	33	28	36	29	25	25	20	17
260	42	34	30	37	30	26	26	21	18
280	44	36	31	40	32	28	27	22	19
300	47	38	33	42	34	30	29	23	20

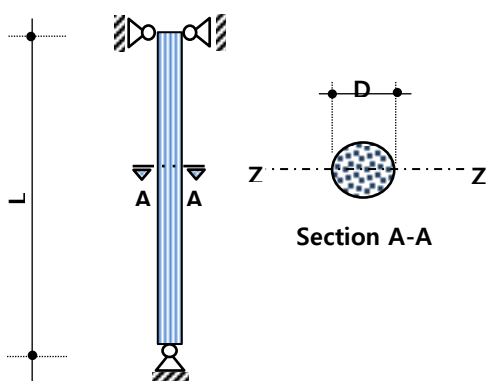


Fig. 10 Rod (column) assuming hinged ends with a circular cross section

Fig. 10 and Euler differential Eq. (4) and behavior of compressive and tensile performance of rods can be changed in moment direction.

$$\sigma_{cr} = \frac{\pi^2 E}{\left(\frac{KL}{r}\right)^2} \quad (3)$$

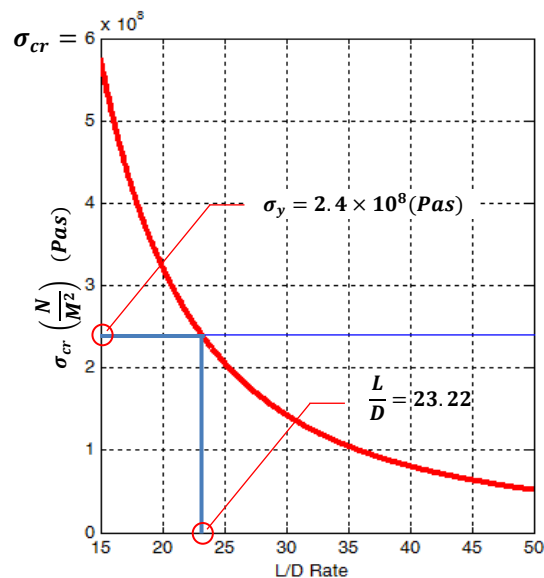
$$\left(A = \frac{\pi D^2}{4} \text{ \& } I_z = I_y = \frac{\pi D^4}{64} \text{ \& } r = \sqrt{\frac{I_z}{A}} \text{ \& } K = 1\right)$$

$$\sigma_{cr} = \frac{\pi^2 D^2 E}{16L^2} = \frac{\pi^2 E}{\left(\frac{4L}{D}\right)^2} \quad (4)$$

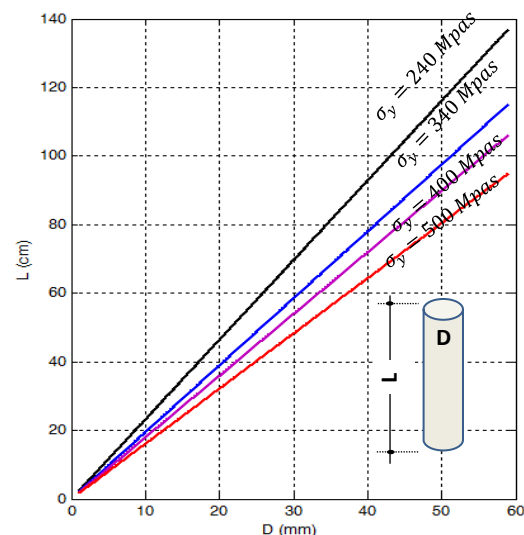
By drawing Eq. (4) (L/D & σ_{cr}) and taking yield stress limit $\sigma_y = 240 \text{ Mpa}$ into account and the elastic modulus $E = 210 \text{ Gpa}$, the ratio L/D was obtained according to Diagram.1 (a) for different types of steel with different σ_y and diameter depending on length, according to Diagram.1 (b).

5. A numerical example

This study focused on a structure composed of steel columns and lumped mass on top (e.g., Arial water tank) with IPB profile and a fixed connection to the foundation under the specifications and behavior of the steel as shown



(a)



(b)

Diagram 1. (a) ratio L/D for steel $\sigma_y = 240 \text{ Mpa}$, $E = 210 \text{ Gpa}$, (b) D and L of steel rods with different σ_y

in Fig. 11.

5.1 Modeling and analysis with steel rods

The theoretical connection behavior model involved several elements, nodes and constraints as shown in Fig. 12, was exactly modeled, the macro version in OpenSees and micro version in ABAQUS. According to $B = 20 \text{ cm}$, $D = 40 \text{ cm}$, $H \approx 10 \text{ cm}$, $L = 10 \text{ cm}$, $HC = 3.0 \text{ m}$ and specifications of the steel in Fig. 12 and IPB200, diameter of the rods according to Table 1. $\Phi_{\text{bar}} = 35 \text{ mm}$. Fig. 13 displays the adoption of two rods on both sides of the connection, $N = 2$ and pushover analysis on macro and micro modes and comparative pushover analysis for the base shear and axial forces in the rods. The results of macro analysis in ABAQUS and OpenSees demonstrated an acceptable consistency of elastic and non-elastic behaviors, except that the computing costs at the same specifications

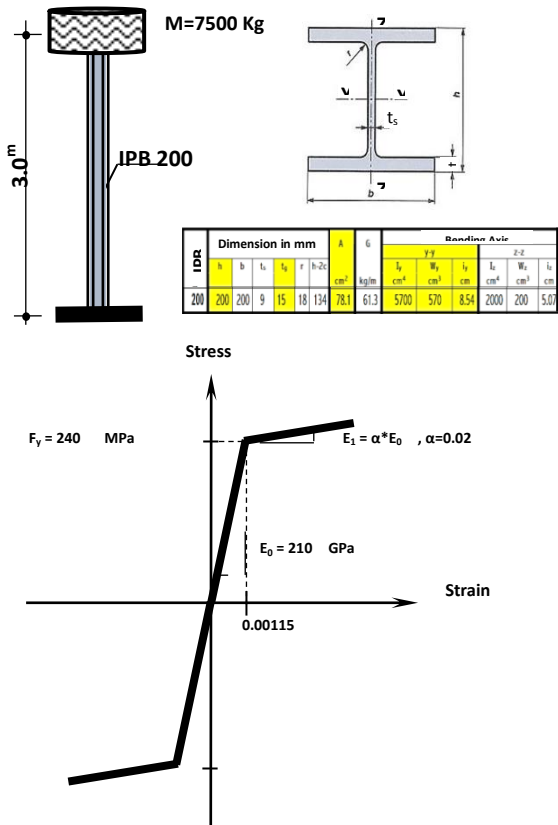


Fig. 11 Structure (column) with a lumped mass and geometric specification and steel behavior

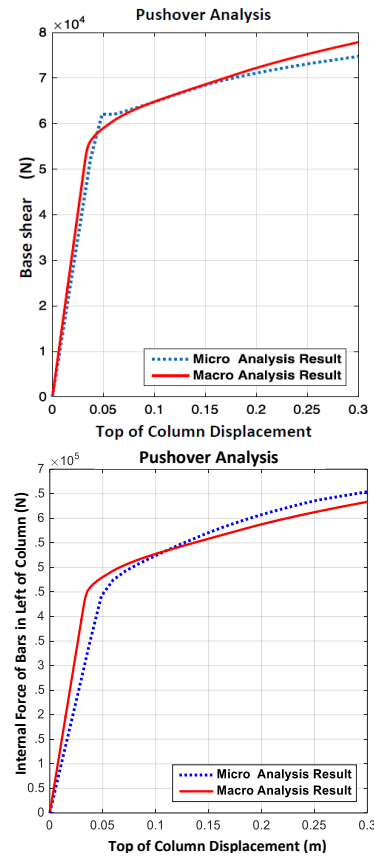


Fig. 13 Pushover analysis results comparison in micro and macro connection model

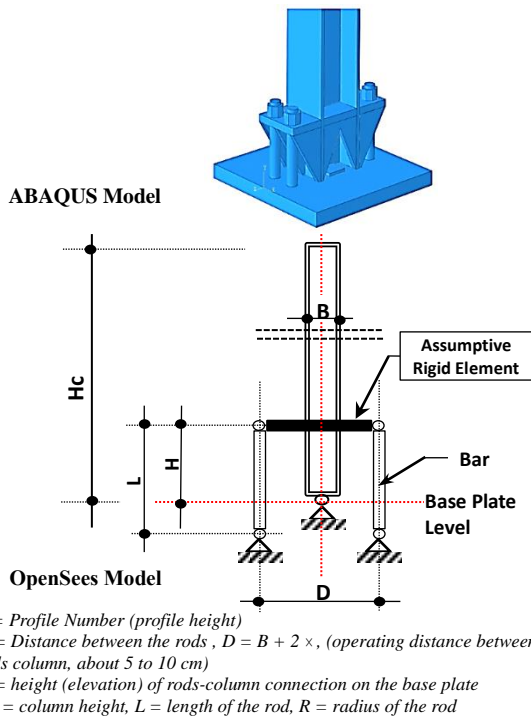
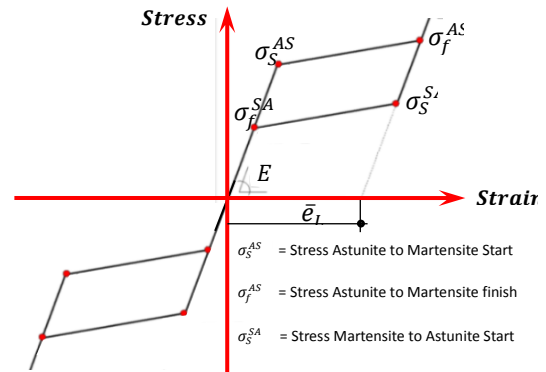


Fig. 12 Theoretical connection model and versions in OpenSees and ABAQUS



Supperelastic Shape Memory Alloy (NiTi)		Mechanical Properties
Astunite Phase	Martensite Phase	
50	50	Elastic Modulus (Gpa)
$\sigma_{st}^{AS} = 400$	$\sigma_{st}^M = 200$	Yield Stress (Mpa)
$\sigma_f^{AS} = 650$	$\sigma_f^M = 50$	
6%	6%	Elastic Strain (%)

Fig. 14 Superelastic stress-strain curve for Nitinol shape memory alloy rods

had a very distinct difference by about 2,000 times so the next sections in this paper performed all the analysis and numerical calculations through OpenSees.

5.2 Modeling and analysis with SMA's equipped rods (superelastic Nitinol)

Table 2 Specifications of Nitinol shape memory alloy (Desroches *et al.* 2004)

Property	NiTi SMA	
	Austenite	Martensite
Physical properties		
Density	6.45 g/cm ³	
Mechanical properties		
Recoverable elongation	up to 8%	
Young's modulus	30-83 GPa	21-41 GPa
Yield strength	195-690 MPa	70-140 MPa
Ultimate tensile strength	895-1,900 MPa	
Elongation at failure	5-50% (typically 25%)	
Poisson's ratio	0.33	
Chemical properties		
Corrosion performance	Excellent (similar to stainless steel)	

The steel rods were removed from the connection and replaced with shape memory alloy (superelastic Nitinol). For this purpose, the behavior of shape memory alloy and mechanical properties with similar behavior in tension and compression, shown Fig. 14 were considered.

6. Designing the equivalent superelastic (Nitinol) SMA rod

Assuming the shape memory rods performs in a way to provide the yield force of steel rods and equivalent stiffness, a relationship can be obtained between shape memory rods and the equivalent steel rods (Fugazza 2005). Assuming the axial stiffness of the rod at $K_{\Delta}=(E \times A) / L$ and axial force of yield for steel rod at $F_y=\sigma_y \cdot A$ and selecting the classic superelastic shape memory alloy rod given the rod type and manufacturer, the modulus of elasticity E^{SMA} is determined. With respect to its characteristics and Fig. 15, the onset stress in austenite to martensite phase is determined in terms of σ_s^{AS} . Hence, the cross section area and diameter of the shape memory alloy rod were calculated according to Eq. (5).

$$A_{Min}^{SMA} = \frac{F_y}{\sigma_s^{AS}} = \frac{\sigma_y}{\sigma_s^{AS}} \times A \quad \& \quad \Phi_{Min}^{SMA} = \sqrt{\frac{4}{\pi} \times \frac{\sigma_y}{\sigma_s^{AS}} A} \quad (5)$$

$$A_{Max}^{SMA} = \frac{F_y}{\sigma_f^{AS}} = \frac{\sigma_y}{\sigma_f^{AS}} \times A \quad \& \quad \Phi_{Max}^{SMA} = \sqrt{\frac{4}{\pi} \times \frac{\sigma_y}{\sigma_f^{AS}} A}$$

By substituting the parameters in Eq. (5) and the connection rod under studying $\Phi_{Bar}=35^{mm}$, the diameter of SMA rod was equal to $\Phi_{Min}^{SMA}=21^{mm}$. Referring to Diagram 1 and selecting a stress curve such as $\sigma_{fAS}=650$ Mpa, the maximum equivalent buckling length of the rod was obtained to be $L=35^{cm}$. Given the sensitivity of the connection behavior to the selective SMA rods and free choice of rod length lower than 35^{cm} , the connection response was examined under different seismic loads, as well as different lengths of connection rods.

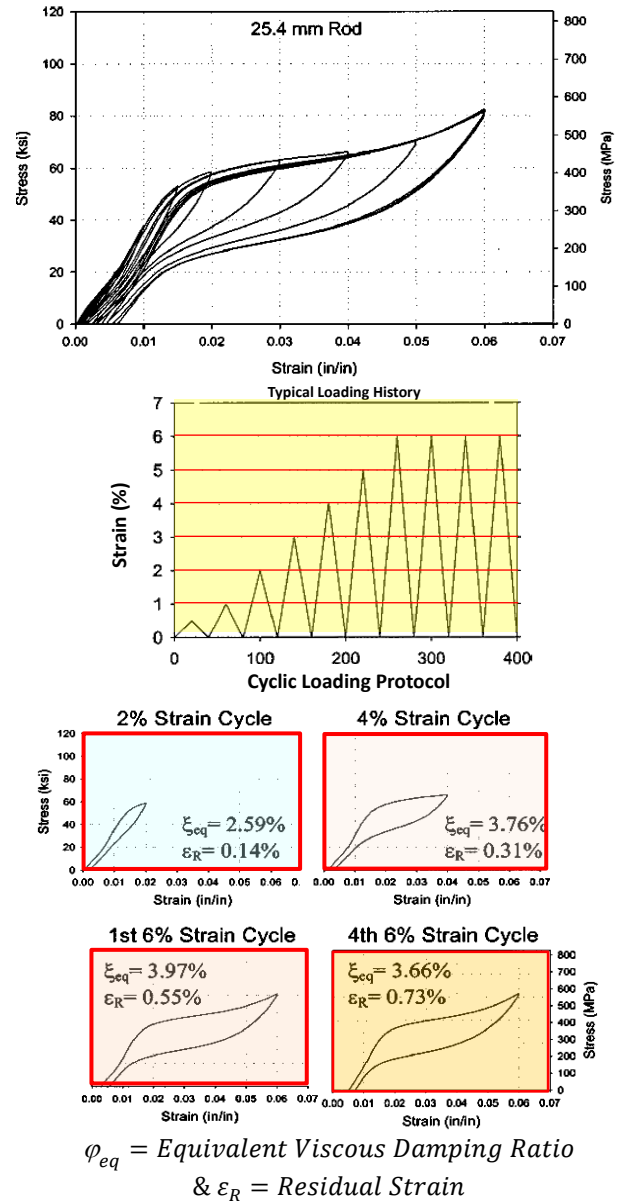


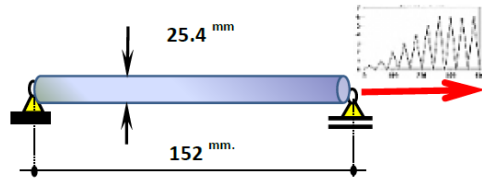
Fig. 15 Stress-Strain behavior curve for 25.4 mm NiTi rod under quasi-static load (Desroches *et al.* 2004)

7. Verification of software results in modeling the Superelastic Rods

An experiment test was conducted on the superelastic properties of Nitinol wire and shape memory alloy rods, the results of which have been explored below (Desroches *et al.* 2004). The samples were tested with the properties shown in Table 2. A number of samples with different diameters up to 25.4^{mm} were tested.

The loading involved a cyclic strain of 1% to 5% at increase by 1% and four 6% cycle at frequency of 0.025 Hz, nearly equivalent to 0.3% per second strain used for the first series of tests. The loading protocols and the results are shown in Fig. 15.

The software modeling involved rods and results of modeling and testing conducted by Desroches *et al.* (2004), and results comparison have been given in Fig. 16.



Model for testing in OpenSees

```

uniaxialMaterial SMA $SMA $E
$eps $SAMS $SAMf $SMAs $SMaf;
section fiberSec 1 {patch circ
1 $VAR $VAR 0.0 0.0 0.0 $R 0.0
360.}
element nonlinearBeamColumn 1 1
2 $VAR 1 1
    
```

Model Code in OpenSees

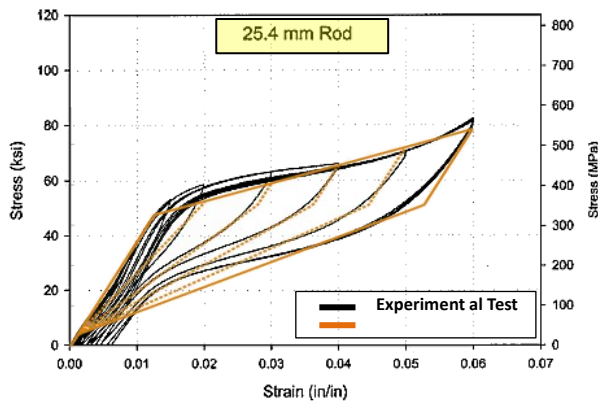


Fig. 16 Modeling and Comparison of testing results conducted by Desroches, *et al* and Opensees model

8. Research methodology

After verification of the application, the structure shown in Fig. 11 was evaluated. Given the mechanical behavior of steel Fig. 12 and mechanical properties of shape memory rods, Table 2, the diameters were calculated according to Eq. (5) and the buckling length was also obtained according to Fig. 1. Moreover, the details of the macro structure and connection were simultaneously modeled in the software as shown in Fig. 13. The structure was initially exposed to cyclic loading and then earthquake records of Elcentro, Tabas, Luma and Northridge. The results in the two scenarios with and without SMA connections were analyzed at different lengths in the software and then the results were compared with each other.

8.1 Cyclic loading analysis

Cyclic loading was used according to protocol AISC 2005 similar to nearby areas in SAC 2000. This loading protocol was proposed by the Institute for Steel Structures for testing fixed end beam-column connections in moment frames. This protocol involves middle story rotational drift, where 6 cycles are in $\theta=0.00375^{\text{rad}}$, 6 cycles in $\theta=0.005^{\text{rad}}$, 6 cycles in $\theta=0.0075^{\text{rad}}$, 4 cycles in $\theta=0.01^{\text{rad}}$, 2 cycles in $\theta=0.015^{\text{rad}}$, 2 cycles in $\theta=0.02^{\text{rad}}$, 2 cycles in $\theta=0.03^{\text{rad}}$ and 2

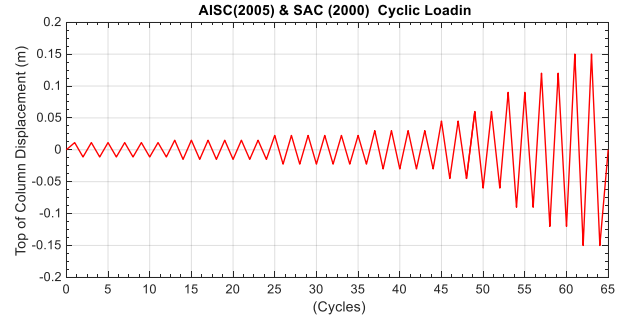


Fig. 17 Cyclic loading protocol for lateral displacement of the column top, AISC 2005 and SAC 2000

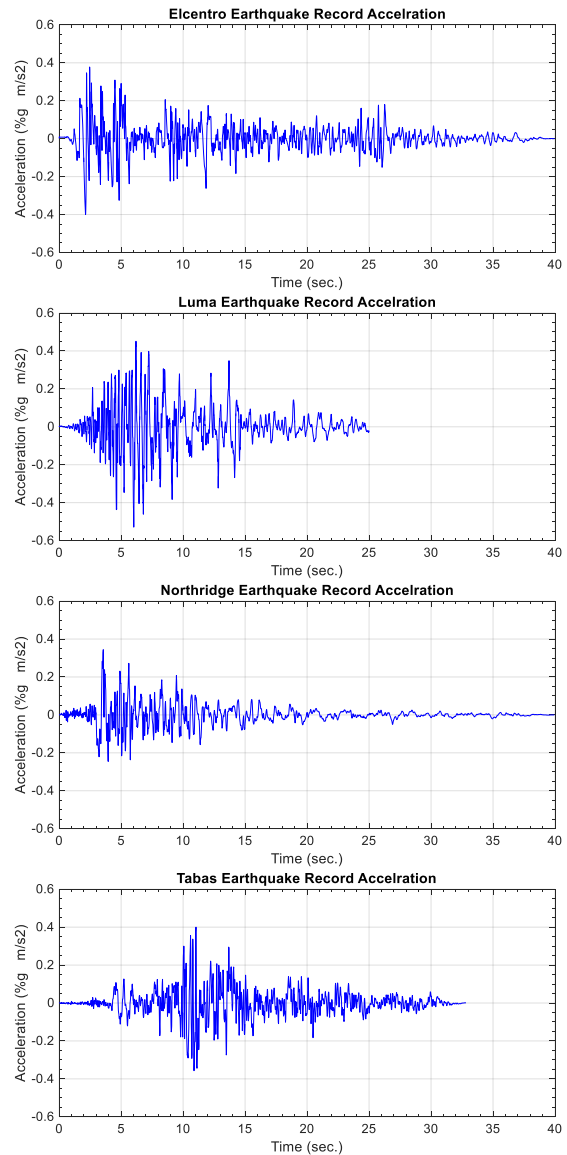
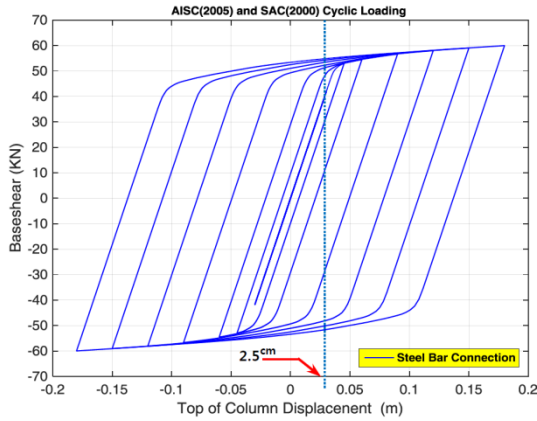


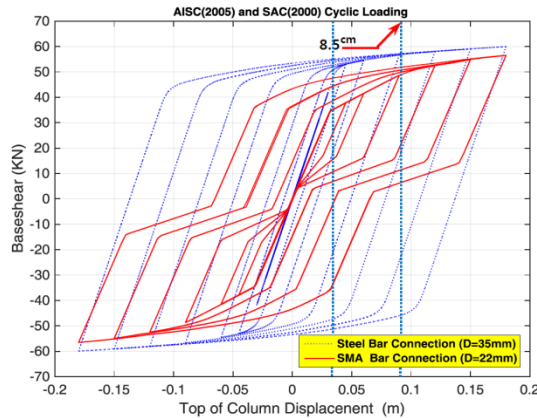
Fig. 18 Earthquake acceleration records under study (Elcentro, Loma, Northridge and Tabas)

cycles in $\theta=0.04^{\text{rad}}$ and the loading per increase of $\theta=0.01^{\text{rad}}$ continues. Given the height of the column $H=3.0^{\text{m}}$ and conversion of rotational drift to lateral drift according to Eq. (6), the lateral displacement was calculated.

Then, the loading protocol for displacement from the top



(a) Response of the connection equipped with Steel bars



(b) Response of the connection equipped with SMA bars and comparison with steel bars

Fig. 19 Hysteresis response of displacement-baseshear under cyclic loading AISC (2005) & SAC (2000)

of the column to $\Delta=20^{cm}$ as in AISC 2005 and Fig. 17 was inserted on the highest point of the column in the software.

$$\theta_{total} = \frac{\Delta}{H} \rightarrow \Delta = \theta_{total} \times H \rightarrow \Delta = \theta \times 3.0^m \quad (6)$$

8.2 Analysis under seismic loading

For seismic loading, the seismic acceleration records of El Centro, Tabas, Loma and Northridge earthquakes were selected from Fig. 18, and then the structure was exposed to base stimulation by the above records so as to extract the analytical results.

9. Results of analysis

9.1 Results of cyclic loading

The results of analyses carried out under cyclic loading and time history response were explored. Figs. 19 and 20 display the carried out results of analyses (hysteresis response of base shear and bars stress versus lateral displacement of top of column) under cyclic loading on top of column with suggested column-foundation connection equipped with steel rods and SMA rods.

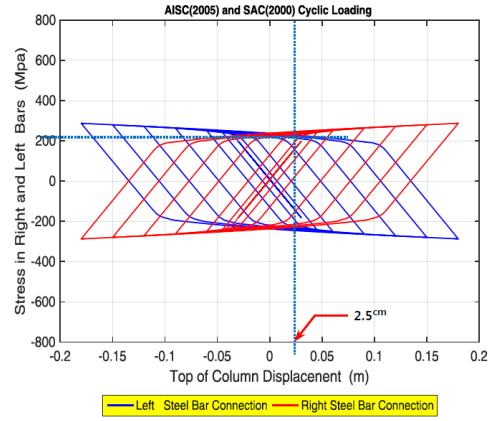


Fig. 20 (a) Hysteresis Response of displacement-stress under cyclic loading AISC (2005) & SAC (2000)

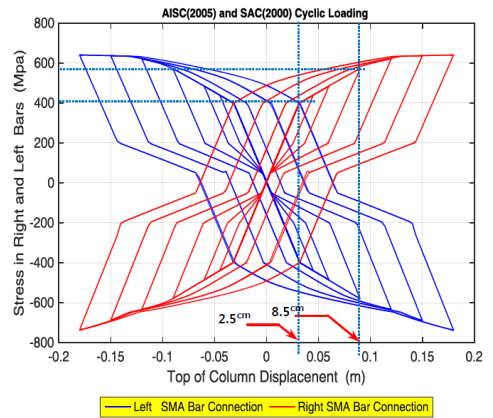


Fig. 20 (b) Hysteresis Response of displacement-stress under cyclic loading AISC (2005) & SAC (2000)

Fig. 19(a) shows baseshear (KN) versus lateral displacement of top of the column (m) due to cyclic loading AISC (2005) & SAC (2000) in column-foundation connection equipped with steel rods. In this connection for lateral displacement equal to 2.5^{cm} (and shearbase equal 45^{KN}) the steel rods have linear elastic behavior and then for lateral displacement upper than 2.5^{cm} the steel rods have nonlinear elastic behavior and residual displacement will have occurred. In the last unloading cycle the residual displacement is near to 13.0^{cm} . Fig. 19(b) shows in column-foundation connection equipped with SMA rods for lateral displacement up to 8.5^{cm} (and shearbase equal 45^{KN}) according to which the SMA rods have linear elastic behavior with various linear behavior (because of phase transformation of austenite to martensite and Vice versa). Although the SMA rods in lateral displacement upper than 8.5^{cm} have linear elastic behavior, column have nonlinear behavior and residual displacement will have occurred. In the last unloading cycle the residual displacement is near to 7.5^{cm} .

Fig. 20(a) shows stress in left and right bars (Mpa) versus lateral displacement of top of the column (m) due to cyclic loading AISC (2005) & SAC (2000) in column-foundation connection equipped with steel rods. In this connection for lateral displacement equal to 2.5^{cm} (and stress equal 240^{MPa}) the steel rods have linear elastic behavior and then for lateral displacement upper than 2.5^{cm}

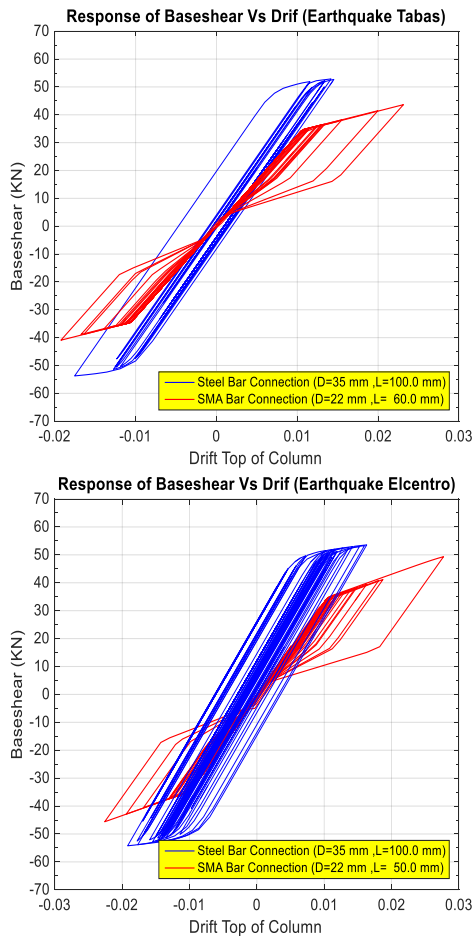


Fig. 21 Comparison hysteresis Response of column top drift and base-shear Under different earthquakes and different connections (with steel rods and SMA Rods)

the steel rods have nonlinear elastic behavior and residual displacement will have occurred as same as Fig. 19(a). Fig. 20(b) shows in column-foundation connection equipped with SMA rods for lateral displacement up to 8.5cm (and stress up to 600Mpa), the SMA rods have linear elastic behavior with various linear behavior and various paths (because of phase transformation of austenite to martensite and Vice versa). Although the SMA rods in lateral displacement upper than 8.5cm have linear elastic behavior, column have nonlinear behavior and residual displacement will have occurred as same as Fig. 19(b). In the last unloading cycle the residual displacement is near to 7.5cm .

9.2 Results of time history loading

Figs. 21 and 22 show obtained analyses results of suggested column-foundation connection (baseshear versus column drift) equipped with steel and SMA rods under the earthquake effects.

Figs. 21 and 22 show hysteresis response of column top drift and baseshear under different selected earthquakes (Tabas, Elcentro, Northridge Luma) and suggested column-foundation connection equipped with steel and SMA rods and their comparison. In all 4 figures, in the suggested connection, the connection equipped with steel rods under

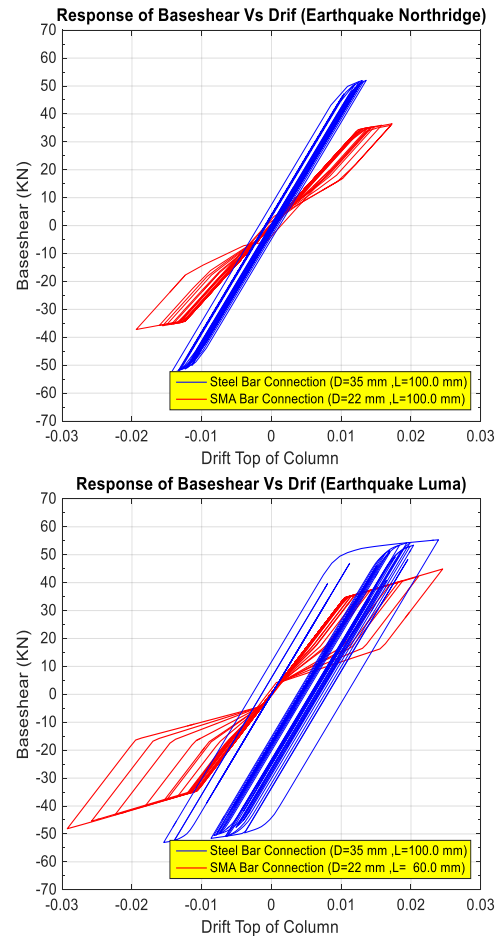


Fig. 22 Comparison hysteresis Response of column top drift and base-shear Under different earthquakes and different connections (with steel rods and SMA Rod)

effect of any selected earthquakes has nonlinear behavior and the connection equipped with SMA rods have linear respons (because of phase transformation of austenite to martensite and Vice versa) with various linear behavior and various paths with an important effect in term of selfcentering.

10. Conclusions

The summary of results obtained from analysis (cyclic and seismic) revealed the following:

- The suggested model for steel column foundation connection showed a behavior fairly consistent with reality. Moreover, it yielded good results in the micro analysis as well as macro.
- Modeling Process shows that connection equipped with/without shape memory alloy bars can be easily modeled in software that analyzes the shape memory elements especially the bars in macro mode and because of conformity to the macro model with the operating model, the suggested connection is easily implemented in the structure, capable of using the exact model in the macro mode.
- By comparing the performances of connection in

cyclic loading based on the protocol, it was observed that Nitinol rods and column deformations had a linear performance over nearly the first 20 cycles and lateral deformation of about 5^{mm} . Having passed the 20th cycle, the non-linear behavior of column experienced and residual deformations occurred, whereas the shape memory rods went through extreme deformation and shift from austenite to martensite phases and vice versa, showed they had self-centring behavior. At the end of the loading cycle, the residual deformations in Fig. 22, concerns the column experiencing non-linear behavior and large residual deformations.

- In examining the performance of connection equipped shape memory alloys and seismic loading, the self-recent ring is obvious because of the shape memory element; so that none of the records affecting the structure and hysteresis curve shown in Fig. 22 indicate any residual deformation in the connection at the end of the analysis.

- In addition to the self-centering of connection equipped with shape memory alloy, there is significant depreciation due to the special behavior of the superelastic Nitinol shape memory alloy as well as frequent shifts from austenite to martensite phases and vice versa on the connection as shown in the hysteresis curve.

- The suggested connection is extremely sensitive to the length and diameter of the rods made of shape memory alloy.

References

- Artar, M. and Daloglu, A.T. (2015), "Optimum design of steel frames with semi-rigid connections and composite beams", *Struct. Eng. Mech.*, **55**(2), 299-313.
- Desroches, R., McCormick, J. and Delemont, M. (2004), "Cyclic Properties of Superelastic Shape Memory Alloy Wires and Bars", *J. Struct. Eng.*, **130**(1), 38-46.
- Desroches, R., Taftali, B. and Ellingwood, B.R. (2010), "Seismic performance assessment of steel frames with shape memory Alloy connections. Part I analysis and seismic demands", *J. Earth. Eng.*, **14**(4), 471-486.
- Fang, C., Yam, M.C.H., Lam, A.C.C. and Xie, L. (2014), "Cyclic Performance of Extended End-plate Connections Equipped with Shape Memory Alloy Bolts", *J. Constr. Steel Res.*, **94**(0), 122-136.
- Fugazza, D. (2005), "Use of shape memory alloy devices in earthquake engineering: mechanical properties, advanced constitutive modeling and structural applications", Ph.D. Dissertation, European School for Advanced Studies. Pavia, Italy.
- Han, Q., Liu, M. and Lu, Y. (2015), "Experimental research on load-bearing capacity of cast steel joints for beam-to-column", *Struct. Eng. Mech.*, **56**(1), 67-83.
- Hu, J.W. and Leon, R.T. (2011), "Analyses and evaluations for composite-moment frames with SMA PR-CFT Connections", *Nonlin. Dyn.*, **65**(4), 433-455.
- Lecce, L. (2015), *Shape Memory Alloy Engineering For Aerospace, Structural and Biomedical Applications*, Elsevier, Italy.
- Leon, R.T., DesRoches, R., Ocel, J. and Hess, G. (2001), "Innovative beam column connections using shape memory

alloys Smart Syst", *SPIE's 8th Annual International Symposium on Smart Structures and Materials*, International Society for Optics and Photonics.

- Ma, H.W., Wilkinson, T. and Cho, C.D. (2007), "Feasibility Study on a Self-centering Beam-to-Column Connection by Using the Superelastic Behavior of SMAs", *Smart Mater. Struct.*, **16**(5), 1555-1563.
- Ocel, J., DesRoches, R., Leon, R.T., Hess, W.G., Krumme, R., Hayes, J.R. and Sweeney, S. (2004), "Steel beam-column connections using shape memory alloys", *J. Struct. Eng.*, ASCE, **130**(5), 732-740.
- Oztekin, E. (2015), "Reliabilities of distances describing bolt placement for high strength steel connections", *Struct. Eng. Mech.*, **54**(1), 149-168.
- Rao, A., Srinivasa, A.R. and Reddy, J.N. (2015), *Design of Shape Memory Alloy (SMA) Actuators*, Springer, London.
- Rofooei, F.R. and Farhidzadeh, A. (2011), "Investigation on the seismic behavior of steel MRF with shape memory alloy equipped connections", *Proceedings of 12th Conference of Structural Engineering. Construction (EASEC12)*, East Asia-Pacific.
- Salari, N. and Asgarian, B. (2015), "Seismic response of steel braced frames equipped with Shape memory alloy-based hybrid devices", *Struct. Eng. Mech.*, **53**(5), 1031-1049
- Saleh, A., Zahrai, S.M. and Mirghaderi, S.R. (2016), "Experimental study on innovative tubular web RBS connections in steel MRFs with typical shallow beams", *Struct. Eng. Mech.*, **57**(5), 785-808.
- Sepulveda, J., Boroschek, R., Herrera, R., Moroni, O. and Sarrazin, M. (2008), "Steel beam-column connection using copper-based shape memory alloy dampers", *J. Constr. Steel Res.*, **64**(4), 429-435.
- Speicher, M.S., Desroches, R. and Leon, R.T. (2011), "Experimental results of a NiTi shape memory alloy (SMA)-based recentering beam-column connection", *Eng. Struct.*, **33**(9), 2448-4457.

CC